

UC Davis

UC Davis Previously Published Works

Title

High-Field EPR Spectroscopic Characterization of Mn(II) Bound to the Bacterial Solute-Binding Proteins MntC and PsaA

Permalink

<https://escholarship.org/uc/item/4zh9b45f>

Journal

The Journal of Physical Chemistry B, 123(23)

ISSN

1520-6106

Authors

Gagnon, Derek M
Hadley, Rose C
Ozarowski, Andrew
[et al.](#)

Publication Date

2019-06-13

DOI

10.1021/acs.jpcc.9b03633

Peer reviewed



HHS Public Access

Author manuscript

J Phys Chem B. Author manuscript; available in PMC 2020 June 13.

Published in final edited form as:

J Phys Chem B. 2019 June 13; 123(23): 4929–4934. doi:10.1021/acs.jpcc.9b03633.

High-Field EPR Spectroscopic Characterization of Mn(II) Bound to the Bacterial Solute-Binding Proteins MntC and PsaA

Derek M. Gagnon¹, Rose C. Hadley², Andrew Ozarowski³, Elizabeth M. Nolan², and R. David Britt¹

¹Department of Chemistry, University of California Davis, Davis, California 95616, United States

²Department of Chemistry, Massachusetts Institute of Technology, Cambridge, Massachusetts 02139, United States

³National High Magnetic Field Laboratory, Florida State University, Tallahassee, Florida 32310, United States

Abstract

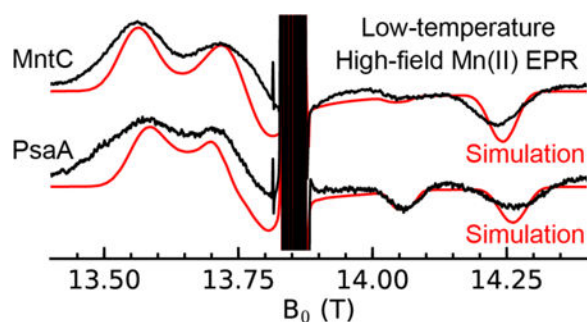
During infection, the bacterial pathogens *Staphylococcus aureus* and *Streptococcus pneumoniae* employ ATP-binding cassette (ABC) transporters to acquire Mn(II), an essential nutrient, from the host environment. Staphylococcal MntABC and streptococcal PsaABC attract the attention of the biophysical and bacterial pathogenesis communities because of their established importance during infection. Previous biophysical examination of Mn(II)-MntC and Mn(II)-PsaA using continuous-wave (≈ 9 GHz) electron paramagnetic resonance (EPR) spectroscopy revealed broad, difficult-to-interpret spectra (Hadley *et al. J. Am. Chem. Soc.* **2018**, *140*, 110–113). Herein we employ high-frequency (>90 GHz), high-field (>3 T) EPR spectroscopy to investigate the Mn(II)-binding sites of these proteins and determine the Spin Hamiltonian parameters. Our analyses demonstrate that the zero-field splitting (ZFS) is large for Mn(II)-MntC and Mn(II)-PsaA at +2.72 and +2.87 GHz, respectively. The measured ⁵⁵Mn hyperfine coupling values for Mn(II)-MntC and Mn(II)-PsaA of 241 and 236 MHz, respectively, demonstrate a more covalent interaction between Mn(II) and the protein compared to Mn(II) in aqueous solution (≈ 265 MHz). These studies indicate that MntC and PsaA bind Mn(II) in a similar coordination geometry. Comparison of the ZFS values determined herein with those ascertained for other Mn(II) proteins suggests that the Mn(II)-MntC and Mn(II)-PsaA coordination spheres are not five coordinate in solution.

Graphical Abstract

Correspondence Inolan@mit.edu, Phone: 617-452-2495. rdbritt@ucdavis.edu, Phone: 530-752-6377.

Supporting Information

Figures S1–S2, simulation parameters for field standards, and EasySpin phenomenological line width inputs used in simulations. This information is available free of charge via the Internet at <http://pubs.acs.org>.



Introduction

Transition metal ions are essential nutrients for all organisms.^{1–2} In the context of bacterial infection, the invading microbe must acquire metal nutrients required for growth and virulence from the host.² These pathogens have evolved several mechanisms to scavenge and import metal ions that include the biosynthesis and deployment of metallophores and the expression of high-affinity metal-uptake proteins.² In this work, we employ high-field electron paramagnetic resonance (EPR) spectroscopy to evaluate the metal-binding properties of two transport proteins that function in the acquisition of Mn(II), a nutrient that is required for high levels of virulence in diverse bacterial pathogens.^{3–5}

Staphylococcus aureus and *Streptococcus pneumoniae* are Gram-positive bacterial pathogens of significant clinical concern because they cause a variety of life-threatening infections.^{6–7} Both organisms employ ATP-binding cassette (ABC) transporters to acquire Mn(II) from the host.^{8–9} These transport systems consist of a membrane-anchored solute-binding protein (SBP) that scavenges Mn(II) from the extracellular environment, a transmembrane permease, and an ATPase located on the cytoplasmic side of the cell membrane.¹⁰ The Mn(II) ABC transporters for *S. aureus* and *S. pneumoniae* are MntABC and PsaABC, respectively. MntC and PsaA are the SBPs that capture Mn(II) and deliver it to the transmembrane permeases of each uptake system.^{11–13}

How MntC and PsaA coordinate Mn(II) and deliver it to their respective permease has not been fully elucidated. Reported crystal structures of Mn(II)-MntC (2.2-Å resolution)¹⁴ and Mn(II)-PsaA (2.7-Å resolution)¹⁵ show Mn(II) bound by a His₂AspGlu coordination sphere in both proteins (Figure 1). The crystallographic Mn(II)-MntC site was described as 5-coordinate where His50, His123, O ϵ 1 of Glu189, and both O δ 1 and O δ 2 of Asp264 coordinate the metal ion (Figure 1B).¹⁴ However, the metal–ligand distances determined crystallographically range from 2.1–2.8 Å and do not preclude the possibility of other coordination geometries (Figure 1). In addition, the metal content of the crystallized protein is ambiguous because the protein in solution contained low amounts of various metal ions according to inductively-coupled mass spectrometry and anomalous diffraction data was not reported,¹⁴ which can be employed to confirm the identity of the bound metal. As a result, the Mn(II) coordination sphere of MntC is not well-defined and requires further examination. The crystallographic Mn(II)-PsaA site was described as 4-coordinate where His67, His139, O ϵ 1 of Glu205 and O δ 1 of Asp280 bind the Mn(II) ion (Figure 1D,E).¹⁵ Nevertheless, the metal–ligand distances determined from this crystal structure range from

2.1–2.4 Å,¹⁵ and the possibility that the bound Mn(II) ion has a higher coordination number cannot be ruled out based on this structural model.⁵ An additional consideration for each SBP is that the coordination geometry or number of the bound Mn(II) ion may change as the SBP delivers Mn(II) to the transmembrane permease. In an effort to gain further insight into these systems, we recently examined the Mn(II) sites of MntC and PsaA by X-band (≈ 9 GHz) EPR spectroscopy.¹⁶ These studies revealed broad spectra resulting from the high magnitude of the zero-field splitting ($|D|$) relative to the spectrometer frequency ($|D|/h\nu \approx 0.3$).¹⁶ As a consequence, the Spin Hamiltonian parameters could not be accurately determined.

In this work, we further investigate the electronic structure of Mn(II)-MntC and Mn(II)-PsaA in the “high-field regime” where $|D| \ll h\nu$ by employing high-field (>3 T) and high-frequency (>90 GHz) EPR spectroscopy. In this regime, the spectra become simplified and simulation of the data can afford values for the Spin Hamiltonian parameters. The spectral data and simulations indicate that MntC and PsaA both bind Mn(II) in a similar tetrahedral or trigonal prismatic coordination environment consistent with the primary coordination sphere defined by the His₂AspGlu motifs observed crystallographically.^{14–15, 17}

Experimental and Theoretical Methods

Sample Preparation.

MntC and PsaA were overexpressed, purified, demetalated, and stored as described previously.¹⁶ All EPR samples were buffer exchanged into 75 mM HEPES, 100 mM NaCl, pH 7.5 that was prepared using high-purity buffer reagents as described elsewhere.¹⁶ For D-band analyses (130 GHz) of the Mn(II)-SBPs, samples of SBP (1 mM) were incubated with Mn(II) (750 μ M) for ≈ 15 min before an approximately 15- μ L aliquot was transferred to a D-band tube (0.50 \times 0.60 mm ID \times OD quartz capillary tubing supplied by Vitrocom) and frozen in liquid nitrogen. These samples were prepared at MIT and shipped to the CalEPR facility at University of California, Davis in a liquid nitrogen dewar. For high-frequency (388 GHz) analyses, MntC (1.2 mM) was incubated with Mn(II) (900 μ M) for ~ 15 min before a 500 μ L aliquot was transferred to a 1 mL LDPE sample vial (Fischer) and frozen in liquid nitrogen. PsaA (2.4 mM) was incubated with Mn(II) (1.8 mM) for ~ 15 min before 500 μ L was transferred to a 1 mL LDPE sample vial (Fischer) and frozen in liquid nitrogen. These samples were shipped to the National High Magnetic Field Laboratory (NHMFL) Electron Magnetic Resonance facility on dry ice.

EPR Measurements.

Pulse spectra at 130 GHz were collected at the University of California, Davis CalEPR facility utilizing a D-band (130 GHz) spectrometer described previously.¹⁸ Spectra were collected at 15 K, with a 20 ns $\pi/2$ pulse length, a τ value of 300 ns, and 1 ms repetition time. The field axis was calibrated by collecting a spectrum of Mn(II) impurity in MgO ($>95\%$ fused MgO, Aldrich). The Mn(II) in MgO signal has a g value of 2.00100(5) and ⁵⁵Mn hyperfine of $-243.6(5)$ MHz.^{19–20}

Spectra collected at the NHMFL were collected utilizing a spectrometer described previously.²¹ The field was calibrated with an internal sample standard of H-atom trapped in an octaisobutylsilsesquioxane nanocage with a g value of 2.00294(3) and hyperfine of 1413.7(1) MHz.¹⁹ Spectra were collected at multiple temperatures with different modulation amplitudes to enhance the intensity of different m_s transitions.

The field calibration with both the external Mn(II) impurity in MgO and internal H-atom standards was carried out during post-processing of the data. Briefly, the general procedure involved manually aligning a simulation of the standard with the experimental data of the field standard by both an initial visual inspection and a subsequent mathematical process. Example inputs for simulations of the standards are included in the Supporting Information. For the Mn(II) impurity in MgO standard, the lowest field hyperfine peak was selected for the initial alignment. After initial visual alignment, the fine adjustment was carried out by calculating the field difference between simulated and experimental field positions for the maximum intensity of the first hyperfine line. We found that this procedure afforded a satisfactory result where all six hyperfine lines of the Mn(II) impurity in MgO lined up. The calculated offset was then used as a field offset factor for the experimental data prior to simulation. The internal hydrogen atom standard required an entirely visual-inspection alignment of the simulation and experimental data due to distortions of the line shape caused by passage and modulation effects during data collection.

EPR Theory and Simulations.

The EPR spectrum of the d^5 Mn(II) ($S = 5/2$) ion can be interpreted using the phenomenological spin Hamiltonian given below.^{22–23}

$$\hat{H} = \frac{\beta_e}{h} B \cdot g \cdot \hat{S} + a_{iso} \hat{S} \cdot \hat{I} + D(\hat{S}_z^2 - S(S+1)/3) + E(\hat{S}_x^2 - \hat{S}_y^2)$$

Where β_e is the Bohr magneton, B is the magnetic field, g is the electron g -value, S the electron spin, h is the Planck constant, a_{iso} is the isotropic and hyperfine interaction with the ^{55}Mn ($I = 5/2$, 100% abundance) nucleus, I is the nuclear spin, D and E are the axial and rhombic zero-field splitting values, respectively. The ratio E/D is reported to indicate the rhombicity of the zero-field splitting tensor. When the coordinate frame is chosen correctly, the values of E/D range from 0 (perfectly axial) to 1/3 (maximally rhombic). All spectra were simulated using the freely available EasySpin (v5.2.24) toolbox for MATLAB R2017a (The Mathworks, Inc.).²⁴

The ^{55}Mn hyperfine values and g -values were determined from simulations of the data collected at temperatures ~ 10 K and assessed by visual inspection. The zero-field splitting values D and E were determined by simulating the data collected at temperatures ~ 5 K. The asymmetry of the spectrum, from which the sign of D can be determined, depends on the magnitude of the Zeeman term rather than on the magnitude of D , and thus is most convincingly observed at the lowest temperatures and highest fields. We found that the relative peak intensities of simulations at high fields and low temperature (~ 5 K) were sensitive to the temperature employed in the simulation. In order to improve the agreement

between the simulation and experimental data, it was necessary to set the simulation temperature 2 K higher than the temperature reported by the spectrometer to achieve the correct relative intensities of the different transitions. The simulation temperature is not expected to affect the measured zero-field splitting parameters, but it affects the relative peak intensities in the simulations. The 388 GHz and 400 GHz Mn(II)-MntC spectrum collected at 3 K were simulated using a temperature of 5 K. The 388 GHz Mn(II)-PsaA spectrum collected at 5 K was simulated using a temperature of 7 K. We note that the recorded spectrometer temperature is not from a temperature probe located at the sample, and that there may be heating of the sample induced by the field modulation during the experiment. D and E strains of 300 MHz were used to help the simulation lineshape better match the linewidths of the experimental data.

Results and Discussion

The EPR spectra of Mn(II)-MntC and Mn(II)-PsaA feature a six-line pattern at $g \cong 2.001$ (4.64 T at 130 GHz, 13.86 T at 388 GHz) that arises from the transition between $m_s = \pm 1/2$ electron spin manifolds and their hyperfine couplings to the ^{55}Mn nucleus ($I = 5/2$, 100% abundance) (Figures 2–4 and S1). Surrounding this central sextet is a broad envelope of transitions belonging to the $m_s = \pm 3/2$ and $m_s = \pm 5/2$ manifolds where the ZFS and strain in those manifolds results in relatively featureless spectra with no resolved ^{55}Mn hyperfine couplings.³⁵ Simulation of the spectra in the sextet region affords ^{55}Mn isotropic hyperfine values of 241 and 236 MHz for Mn(II)-MntC and Mn(II)-PsaA, respectively (Table 1). The relatively low ^{55}Mn hyperfine constant values indicate a more covalent interaction of the $S = 5/2$ Mn(II) ion with its ligands in the binding site of the protein compared to hexa-aqua Mn(II), for which the ^{55}Mn hyperfine value is ≈ 265 MHz.²² This more covalent interaction combined with the electrostatic interaction from the negatively charged carboxylate groups of the His₂AspGlu binding site likely contributes to the tight binding of the Mn(II) ion ($K_{d,\text{Mn(II)}} = 10 \text{ nM}$)^{14–15} observed for these two proteins. The simulation also affords isotropic g -values of 2.0011 and 2.0007 for MntC and PsaA, respectively. The isotropic nature of g and the ^{55}Mn hyperfine is expected from the spherically symmetrical unpaired electron spin density of the high spin ($S = 5/2$) d^5 ground state of the Mn(II) ion with no low-lying excited states.

The zero-field splitting parameters D and E/D are best measured in the high-frequency/field spectra. At these high fields, and at low temperatures (<6 K), the lower Zeeman energy $m_s = -5/2$ and $-3/2$ levels become preferentially populated, leading to an increased intensity of the $m_s = -5/2 \leftrightarrow -3/2$ and $-3/2 \leftrightarrow -1/2$ transitions relative to the other transitions (Figures 5, 6 and S2). Simulation afforded values for D (E/D) of +2.72 GHz (0.177) and +2.87 GHz (0.122) for Mn(II)-MntC and Mn(II)-PsaA, respectively (Table 1). The ability to determine the magnitude and sign of D from high-field EPR spectroscopy allows comparisons to other spectroscopically and structurally characterized systems. The values of $|D|$ determined for Mn(II)-MntC and Mn(II)-PsaA are intermediate between the relatively high values reported for the 5-coordinate superoxide dismutases (SODs) and the remarkably low values reported for the nearly idealized octahedral Mn(II) coordination spheres in human and murine calprotectin (Table 1).^{26, 33–34} Moreover, the sign of D is positive for the Mn(II)-SBPs and negative, when reported, for MnSOD.²⁵ Taken together, these comparisons suggest that the

Mn(II)-SBP sites are neither 5-coordinate nor highly symmetrical 6-coordinate species. Moreover, the zero-field splitting parameters for the Mn(II)- SBPs show the greatest similarity to the 6-coordinate trigonal prismatic Mn(II) site displayed in OxDc site II and the 6-coordinate bacterial reaction center from *Rhodobacter spheroides*.^{27–28} Thus, it is possible that the Mn(II)-SBP sites are 6-coordinate. However, we note that caution must be taken when using the magnitude of the Mn(II) zero-field splitting parameter D to infer coordination geometry. The comparison should only be done with similar ligand types since the identity of the ligands can influence the zero-field splitting.^{36–38} We also note that there is a paucity of zero-field splitting parameters determined for known tetrahedral Mn(II) complexes reported in the literature. To the best of our knowledge, this work is currently limited to Mn(II) complexes containing halide ligands,³⁹ which are inappropriate comparisons for the Mn(II)-SBPs because halide ligands affect the ZFS.^{37–38, 39} Thus, we are unable to determine how similar or different the Mn(II) zero-field splitting parameter values of the Mn(II)-SBPs are to known tetrahedral Mn(II) species. Nevertheless, both Mn(II)-MntC and Mn(II)-PsaA exhibit similar spectroscopic parameters, which suggests that these two Mn(II) sites exhibit more similar coordination environments than indicated by interpretations and comparisons of the Mn(II)-MntC (5- coordinate)¹⁴ and Mn(II)-PsaA (4-coordinate)¹⁵ crystal structures.

Conclusion

The high similarity in the Spin Hamiltonian parameters determined for Mn(II)-MntC and Mn(II)-PsaA suggests that the Mn(II) coordination spheres of these two SBPs are nearly identical in solution. Based on comparisons to previously characterized Mn(II) proteins, the current data suggest that the Mn(II) sites of both proteins are not five coordinate; however, more information on Mn(II) complexes of known coordination geometries is needed to further substantiate this possibility and ascertain whether the SBPs coordinate Mn(II) in a tetrahedral or 6-coordinate manner. Thus, we reason that both SBPs release and deliver Mn(II) to their respective permeases in a similar manner. Indeed, elucidating the molecular mechanism by which the fully reconstituted transport systems MntABC and PsaABC capture Mn(II) with high affinity and deliver the ion to the bacterial cytoplasm is an important and intriguing avenue for future investigation.

Supplementary Material

Refer to Web version on PubMed Central for supplementary material.

Acknowledgments

We gratefully acknowledge financial support from the National Institute of Health grants R35GM126961 (R.D.B) and R01GM118695 (E.M.N.). The work performed at the National High Magnetic Field Laboratory is supported by the National Science Foundation Cooperative Agreement No. DMR-1644779 and the State of Florida.

References

1. Waldron KJ; Rutherford JC; Ford D; Robinson NJ Metalloproteins and metal sensing. *Nature* 2009, 460, 823–830. [PubMed: 19675642]

2. Hood MI; Skaar EP Nutritional immunity: transition metals at the pathogen–host interface. *Nat. Rev. Microbiol* 2012, 10, 525–537. [PubMed: 22796883]
3. Papp-Wallace KM; Maguire ME Manganese transport and the role of manganese in virulence. *Annu. Rev. Microbiol* 2006, 60, 187–209. [PubMed: 16704341]
4. Juttukonda LJ; Skaar EP Manganese homeostasis and utilization in pathogenic bacteria. *Mol. Microbiol* 2015, 97, 216–228. [PubMed: 25898914]
5. Brophy MB; Nolan EM Manganese and microbial pathogenesis: sequestration by the Mammalian immune system and utilization by microorganisms. *ACS Chem. Biol* 2015, 10, 641–651. [PubMed: 25594606]
6. Kobayashi SD; Malachowa N; DeLeo FR Pathogenesis of *Staphylococcus aureus* abscesses. *Am. J. Pathol* 2015, 185, 1518–1527. [PubMed: 25749135]
7. Kim L; McGee L; Tomczyk S; Beall B Biological and epidemiological features of antibiotic-resistant *Streptococcus pneumoniae* in re- and post-conjugate vaccine eras: a United States perspective. *Clin. Microbiol. Rev* 2016, 29, 525–552. [PubMed: 27076637]
8. Horsburgh MJ; Wharton SJ; Cox AG; Ingham E; Peacock S; Foster SJ MntR modulates expression of the PerR regulon and superoxide resistance in *Staphylococcus aureus* through control of manganese uptake. *Mol. Microbiol* 2002, 44, 1269–1286. [PubMed: 12028379]
9. Dintilhac A; Alloing G; Granadel C; Claverys J-P Competence and virulence of *Streptococcus pneumoniae*: Adc and PsaA mutants exhibit a requirement for Zn and Mn resulting from inactivation of putative ABC metal permeases. *Mol. Microbiol* 1997, 25, 727–739. [PubMed: 9379902]
10. Ma Z; Jacobsen FE; Giedroc DP Coordination chemistry of bacterial metal transport and sensing. *Chem. Rev* 2009, 109, 4644–4681. [PubMed: 19788177]
11. Rajam G; Anderton JM; Carlone GM; Sampson JS; Ades EW Pneumococcal surface adhesin A (PsaA): a review. *Crit. Rev. Microbiol* 2008, 34, 131–142. [PubMed: 18728990]
12. Gribenko AV; Liberator P; Anderson AS; Matsuka YV; Mosyak L Cell surface antigen – manganese-binding protein MntC from *Staphylococcus aureus*. In *Encyclopedia of Inorganic and Bioinorganic Chemistry*, John Wiley & Sons, Ltd: 2015.
13. Eijkelkamp BA; McDevitt CA; Kitten T Manganese uptake and streptococcal virulence. *Biometals* 2015, 28, 491–508. [PubMed: 25652937]
14. Gribenko A; Mosyak L; Ghosh S; Parris K; Svenson K; Moran J; Chu L; Li S; Liu T; Woods VL Jr.; et al. Three-dimensional structure and biophysical characterization of *Staphylococcus aureus* cell surface antigen–manganese transporter MntC. *J. Mol. Biol* 2013, 425, 3429–3445. [PubMed: 23827136]
15. McDevitt CA; Ogunniyi AD; Valkov E; Lawrence MC; Kobe B; McEwan AG; Paton JC A molecular mechanism for bacterial susceptibility to zinc. *PLoS Pathog* 2011, 7, e1002357. [PubMed: 22072971]
16. Hadley RC; Gagnon DM; Brophy MB; Gu Y; Nakashige TG; Britt RD; Nolan EM Biochemical and spectroscopic observation of Mn(II) sequestration from bacterial Mn(II) transport machinery by calprotectin. *J. Am. Chem. Soc* 2018, 140, 110–113. [PubMed: 29211955]
17. Lawrence MC; Pilling PA; Epa VC; Berry AM; Ogunniyi AO; Paton JC The crystal structure of pneumococcal surface antigen PsaA reveals a metal-binding site and a novel structure for a putative ABC-type binding protein. *Structure* 1998, 6, 1553–1561. [PubMed: 9862808]
18. Oyala PH; Ravichandran KR; Funk MA; Stucky PA; Stich TA; Drennan CL; Britt RD; Stubbe J Biophysical characterization of fluorotyrosine probes site-specifically incorporated into enzymes: *E. coli* ribonucleotide reductase as an example. *J. Am. Chem. Soc* 2016, 138, 7951–7964. [PubMed: 27276098]
19. Stoll S; Ozarowski A; Britt RD; Angerhofer A Atomic hydrogen as high-precision field standard for high-field EPR. *J. Magn. Reson* 2010, 207, 158–163. [PubMed: 20813570]
20. Burghaus O; Rohrer M; Göttinger T; Plato M; Möbius K A novel high-field/high-frequency EPR and ENDOR spectrometer operating at 3 mm wavelength. *Meas. Sci. Technol* 1992, 3, Meeting 765–774.

21. Hassan AK; Pardi LA; Krzystek J; Sienkiewicz A; Goy P; Rohrer M; Brunel L-C Ultrawide band multifrequency high-field EMR technique: a methodology for increasing spectroscopic information. *J. Magn. Reson* 2000, 142, 300–312. [PubMed: 10648147]
22. Stich TA; Lahiri S; Yeagle G; Dicus M; Brynda M; Gunn A; Aznar C; DeRose VJ; Britt RD Multifrequency pulsed EPR studies of biologically relevant manganese(II) complexes. *Appl. Magn. Reson* 2007, 31, 321–341. [PubMed: 22190766]
23. Weil JA; Bolton JR *Electron paramagnetic resonance: elementary theory and practical applications* 2 ed.; Wiley-Interscience: Hoboken, N. J., 2007.
24. Stoll S; Schweiger A EasySpin, a comprehensive software package for spectral simulation and analysis in EPR. *J. Magn. Reson* 2006, 178, 42–55. [PubMed: 16188474]
25. Sharma A; Gaidamakova EK; Grichenko O; Matrosova VY; Hoeke V; Klimenkova P; Conze IH; Volpe RP; Tkavc R; Gostin ar C; et al. Across the tree of life, radiation resistance is governed by antioxidant Mn^{2+} , gauged by paramagnetic resonance. *Proc. Natl. Acad. Sci. U. S. A* 2017, 114, E9253–E9260. [PubMed: 29042516]
26. Un S; Dorlet P; Voyard G; Tabares LC; Cortez N High-field EPR characterization of manganese reconstituted superoxide dismutase from *Rhodobacter capsulatus*. *J. Am. Chem. Soc* 2001, 123, 10123–10124. [PubMed: 11592902]
27. Tabares LC; Cortez N; Agalidis I; Un S Temperature-dependent coordination in *E. coli* manganese superoxide dismutase. *J. Am. Chem. Soc* 2005, 127, 6039–6047. [PubMed: 15839704]
28. Angerhofer A; Moomaw EW; García-Rubio I; Ozarowski A; Krzystek J; Weber RT; Richards NGJ Multifrequency EPR studies on the Mn(II) centers of oxalate decarboxylase. *J. Phys. Chem. B* 2007, 111, 5043–5046. [PubMed: 17444678]
29. Gaffney BJ; Su C; Oliw EH Assignment of EPR transitions in a manganese-containing lipoxxygenase and prediction of local structure. *Appl. Magn. Reson* 2001, 21, 413–424. [PubMed: 16518455]
30. Chen Y; Wennman A; Karkehabadi S; Engstrom A; Oliw EH Crystal structure of linoleate 13R-manganese lipoxxygenase in complex with an adhesion protein. *J. Lipid Res* 2016, 57, 1574–1588. [PubMed: 27313058]
31. Meirovitch E; Luz Z; Kalb AJ, Electron spin resonance spectroscopy of aqueous solutions of concanavalin A. *J. Am. Chem. Soc* 1974, 96 (24), 7542–7546. [PubMed: 4372266]
32. Tao L; Stich TA; Butterfield CN; Romano CA; Spiro TG; Tebo BM; Casey WH; Britt RD Mn(II) binding and subsequent oxidation by the multicopper oxidase MnxG investigated by electron paramagnetic resonance spectroscopy. *J. Am. Chem. Soc* 2015, 137, 10563–10575. [PubMed: 26244911]
33. Gagnon DM; Brophy MB; Bowman SEJ; Stich TA; Drennan CL; Britt RD; Nolan EM Manganese binding properties of human calprotectin under conditions of high and low calcium: X-ray crystallographic and advanced electron paramagnetic resonance spectroscopic analysis. *J. Am. Chem. Soc* 2015, 137, 3004–3016. [PubMed: 25597447]
34. Hadley RC; Gagnon DM; Ozarowski A; Britt RD; Nolan EM Murine calprotectin coordinates Mn(II) at a hexahistidine site with Ca(II)-dependent affinity. *Inorg. Chem* 2019, in press.
35. Reed GH; Markham GD EPR of Mn(II) complexes with enzymes and other proteins. In *Biological Magnetic Resonance*, Berliner LJ; Reuben J, Eds. Plenum Press: New York, 1984; Vol. 6, pp 73–142.
36. Walsby CJ; Telser J; Rigsby RE; Armstrong RN; Hoffman BM Enzyme control of small-molecule coordination in FosA as revealed by ^{31}P pulsed ENDOR and ESE-EPR. *J. Am. Chem. Soc* 2005, 127, 8310–8319. [PubMed: 15941264]
37. Duboc C; Phoeung T; Zein S; Pécaut J; Collomb M-N; Neese F Origin of the zero-field splitting in mononuclear octahedral dihalide Mn^{II} complexes: an investigation by multifrequency high-field electron paramagnetic resonance and density functional theory. *Inorg. Chem* 2007, 46, 4905–4916. [PubMed: 17508742]
38. Duboc C; Collomb M-N; Neese F Understanding the zero-field splitting of mononuclear manganese(II) complexes from combined EPR spectroscopy and quantum chemistry. *Appl. Magn. Reson* 2010, 37, 229–245.

39. Wood RM; Stucker DM; Jones LM; Lynch WB; Misra SK; Freed JH An EPR study of some highly distorted tetrahedral manganese(II) complexes at high magnetic fields. *Inorg. Chem* 1999, 38, 5384–5388.
40. Zein S; Duboc C; Lubitz W; Neese F A systematic density functional study of the zero-field splitting in Mn(II) coordination compounds. *Inorg. Chem* 2008, 47, 134–142. [PubMed: 18072763]

Author Manuscript

Author Manuscript

Author Manuscript

Author Manuscript

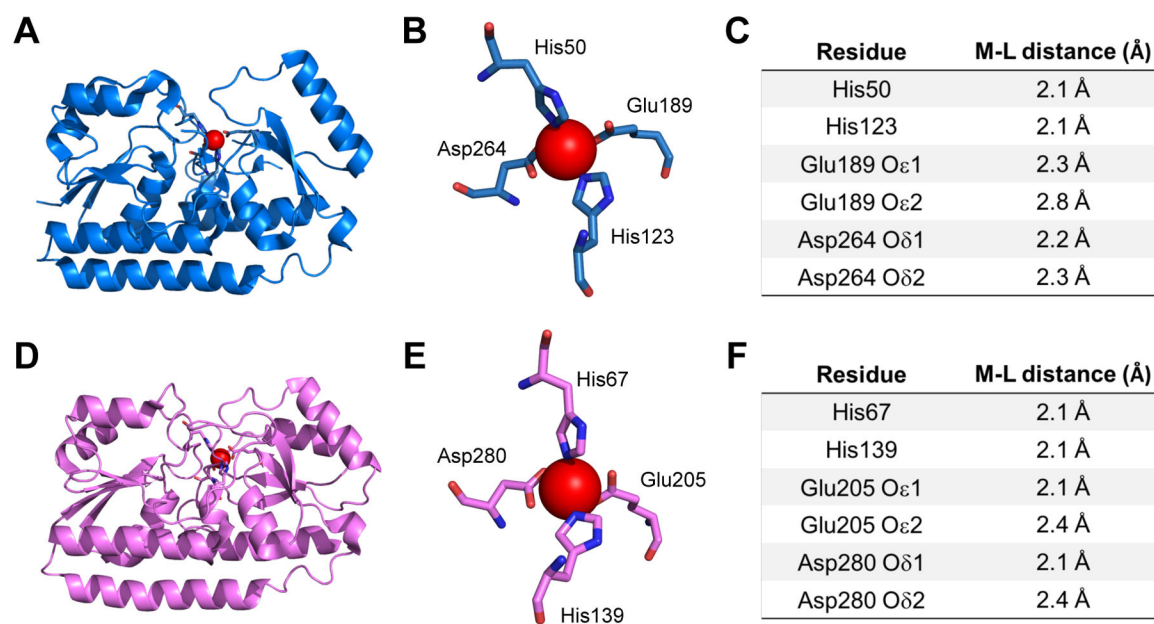


Figure 1.

Crystal structures, zoom-in view of the metal-binding sites, and metal-ligand distances of Mn(II)-MntC (A,B,C; PDB: 4K3V) and Mn(II)-PsaA (D,E,F; PDB: 3ZTT). The Mn(II) ion is shown as a red sphere. Ligand numbering in MntC corresponds to a truncated form of the protein.¹⁴

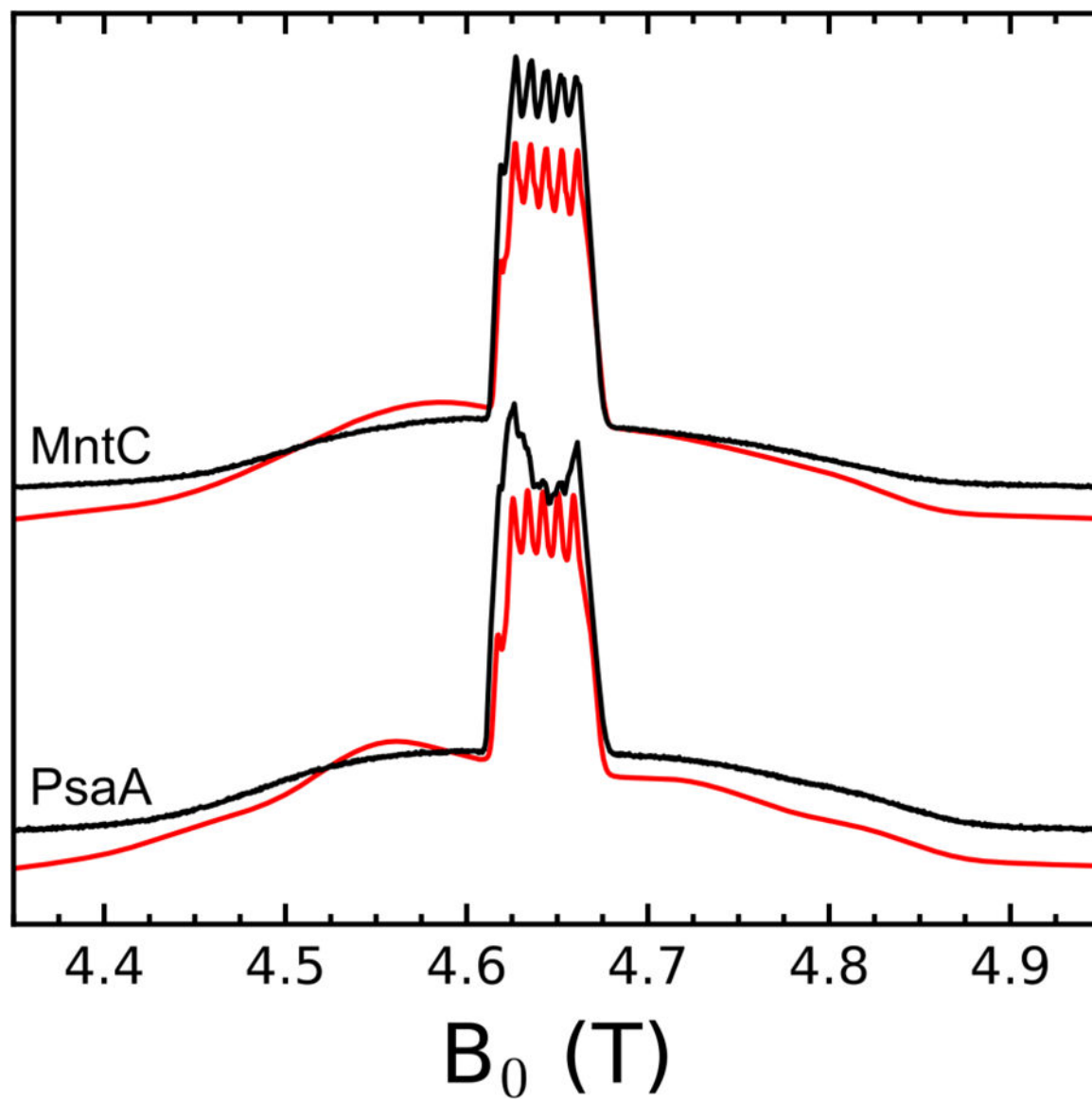


Figure 2.

2p echo-detected field sweep of Mn(II)-MntC and Mn(II)-PsaA at 130 GHz (75 mM HEPES, 100 mM NaCl, pH 7.5). The black traces are the experimental data and the red traces are simulations with the parameters listed in Table 1. Experimental settings: spectrometer frequency 130 GHz, 1 ms rep time, 20 ns $\pi/2$ pulse length, $\tau = 300$ ns, $T = 15$ K. The Mn(II)-PsaA spectrum appears to have a contaminant around ≈ 4.630 – 4.66 T that partially obscures the sextet.

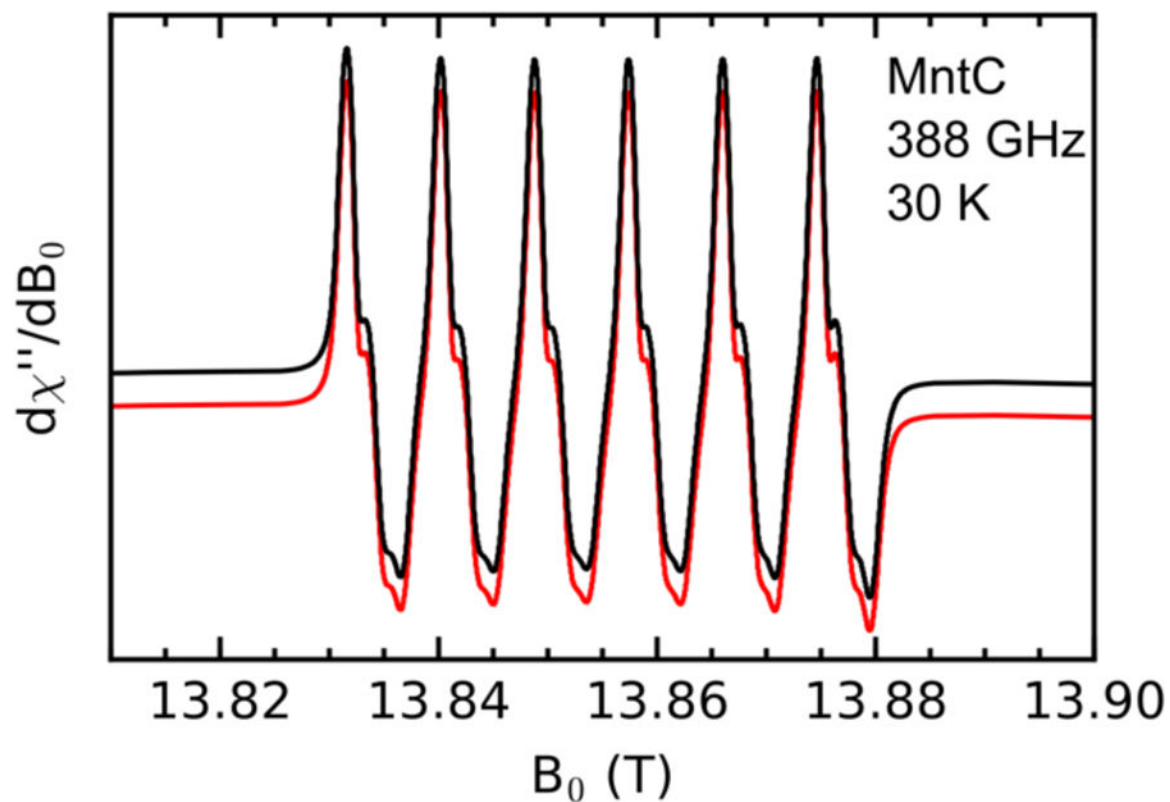


Figure 3. High-field/frequency CW EPR spectrum of Mn(II)-MntC at 388 GHz (75 mM HEPES, 100 mM NaCl, pH 7.5). The black trace is the experimental data and the red trace is a simulation with the parameters listed in Table 1. Experimental settings: spectrometer frequency 388 GHz, 0.5 mT modulation amplitude at 50 kHz, $T = 30$ K.

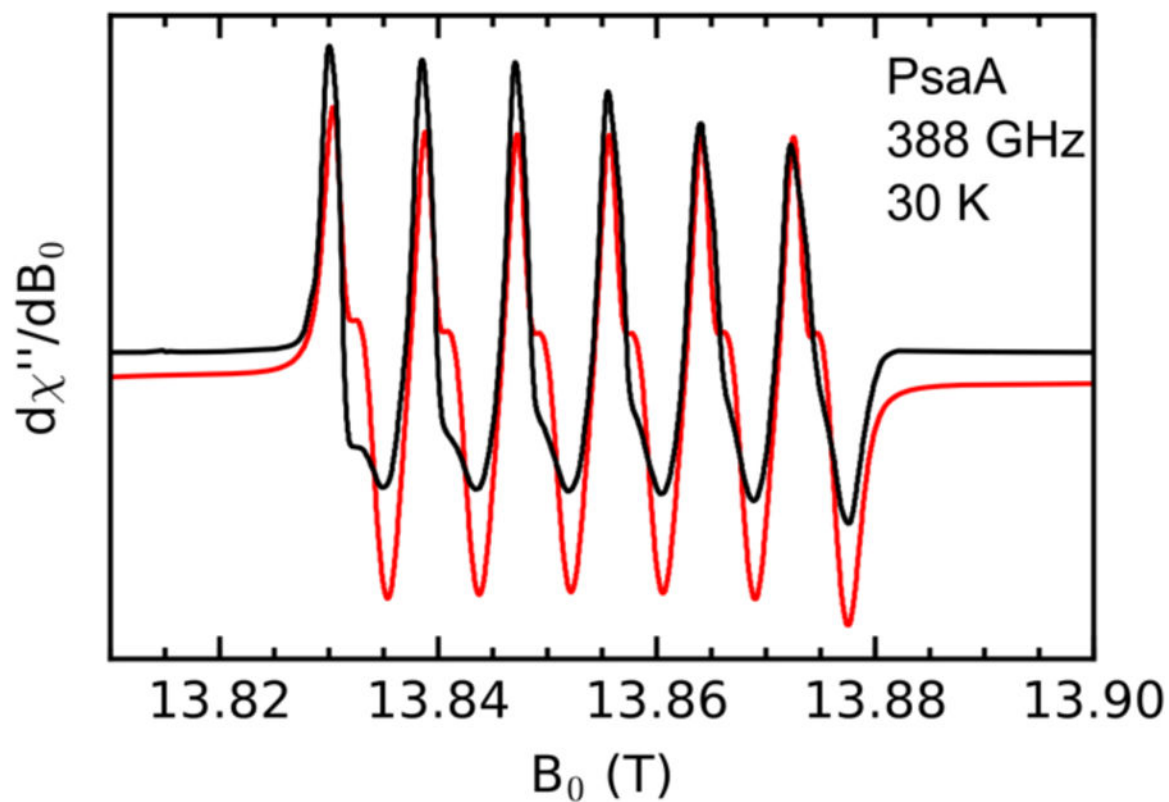


Figure 4. High-field/frequency CW EPR spectrum of Mn(II)-PsaA at 388 GHz (75 mM HEPES, 100 mM NaCl, pH 7.5). The black trace is the experimental data and the red trace is a simulation with the parameters listed in Table 1. Experimental settings: spectrometer frequency 388 GHz, 0.5 mT modulation amplitude at 50 kHz, $T = 30$ K.

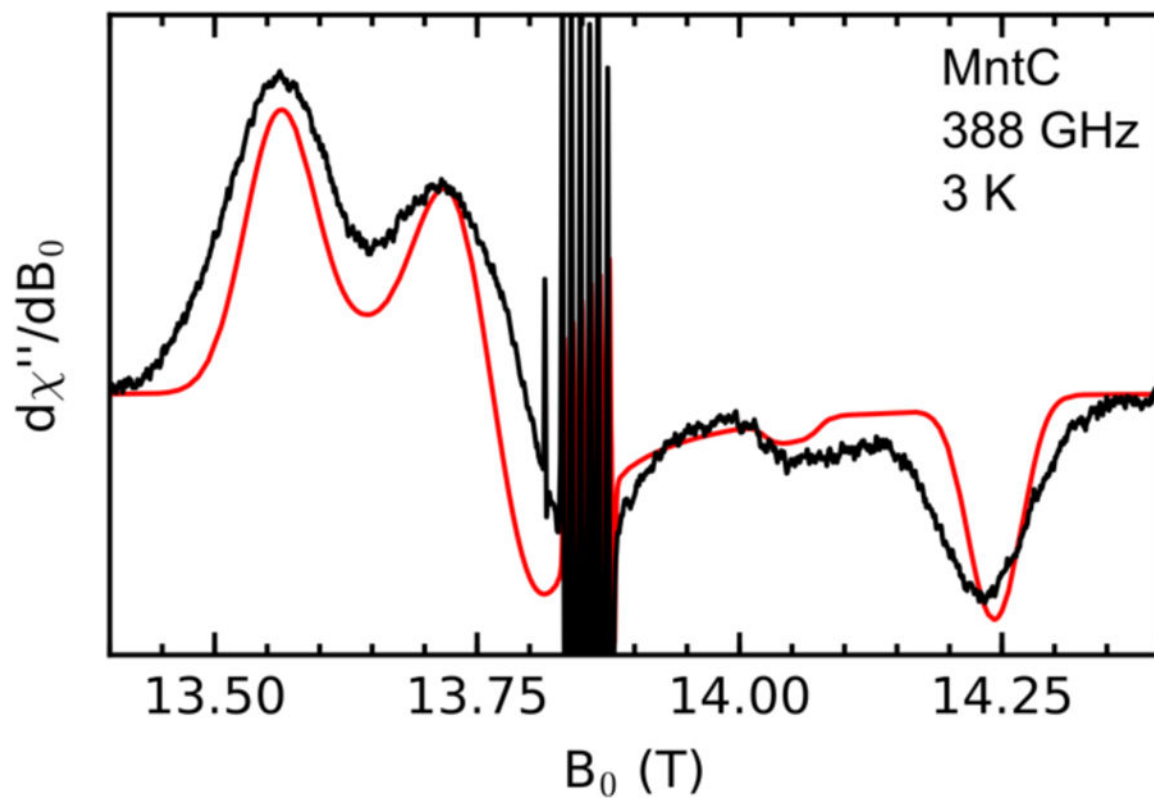


Figure 5. High-field/frequency CW EPR spectrum of Mn(II)-MntC at $T = 3$ K, conditions where the spectrum is dominated by the $-5/2 \leftrightarrow -3/2$ and $-3/2 \leftrightarrow -1/2$ transitions (75 mM HEPES, 100 mM NaCl, pH 7.5). Experimental settings: spectrometer frequency 388 GHz, 2.5 mT modulation amplitude at 50 kHz, $T = 3$ K.

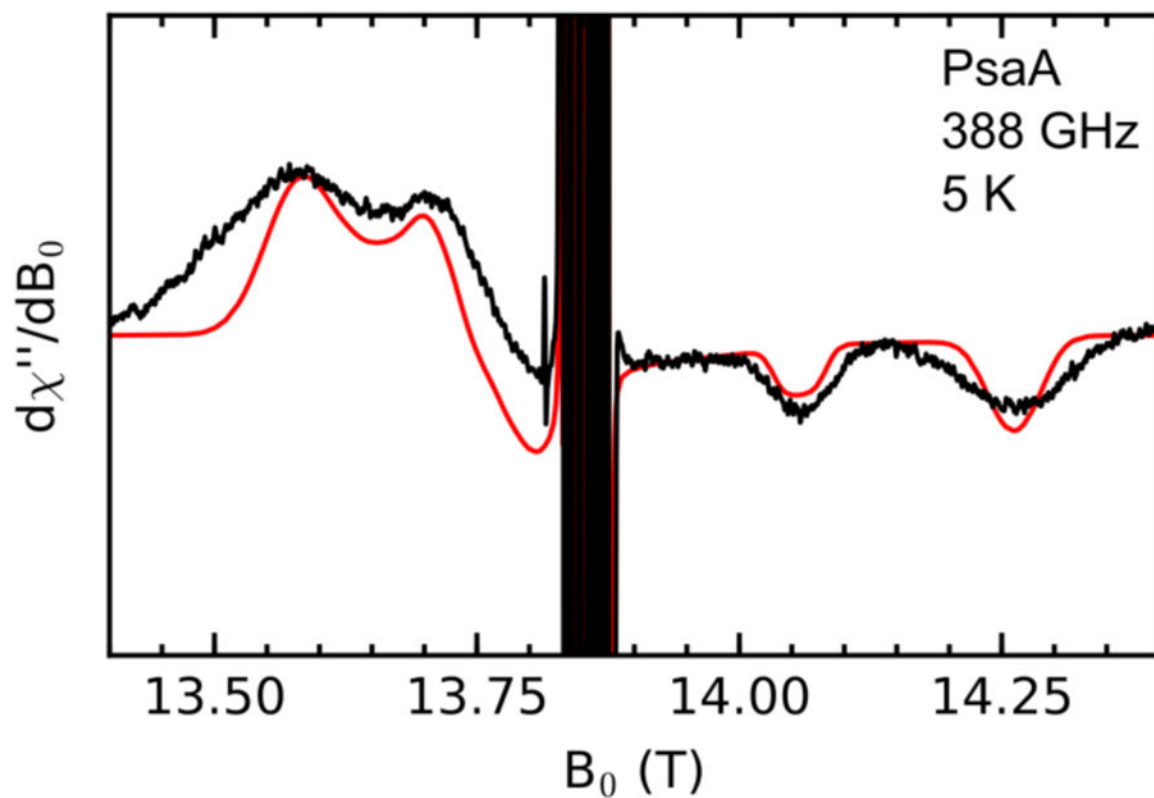


Figure 6.

High-field/frequency CW EPR spectrum of Mn(II)-MntC at $T = 5$ K, conditions where the spectrum is dominated by the $-5/2 \leftrightarrow -3/2$ and $-3/2 \leftrightarrow -1/2$ transitions (75 mM HEPES, 100 mM NaCl, pH 7.5). Experimental settings: spectrometer frequency 388 GHz, 2.4 mT modulation amplitude at 50 kHz, $T = 5$ K.

Table 1.

Table of Spectroscopic Parameters for Mn(II) Bound to Various Proteins

Mn(II)-bound protein	D (GHz) ^a	$ E $ (GHz)	$ E/D $	⁵⁵ Mn a_{iso} (MHz)	Coordination motif ^b	ref
MntC	+2.72(5)	0.48(5)	0.177	241	N ₂ O ₂ or N ₂ O ₄	this work
PsaA	+2.87(5)	0.35(5)	0.122	236	N ₂ O ₂ or N ₂ O ₄	this work
<i>Df</i> MnSOD ^c	-10.490	0.779	0.074	244	N ₃ O ₂	25
<i>Ec</i> MnSOD ^d	10.640	0.853	0.080	230	N ₃ O ₂	26
<i>Ec</i> MnSOD + 0.1 M azide ^d	1.390	0.270	0.194	245	N ₄ O ₂	26
Mn(II) photosynthetic reaction center from <i>R. spheroides</i>	3.328	0.749	0.225	n.d. ⁱ	N ₄ O ₂	27
OxDc site I ^e	1.200	0.250	0.208	253	N ₃ O ₃	28
OxDc site II ^e	2.700	0.675	0.250	250	N ₃ O ₃	28
Lipoxygenase ^f	+2.1-3	0.105-0.540	0.18(0.05)	258	N ₃ O ₃	29,30
concanavalin A	0.645	0.071	0.010	259	N ₁ O ₅	31
Mnx ^g	1.080	0.356	0.329	n.d. ⁱ	N ₁ O ₅	32
Human calprotectin	0.485	0.146	0.30	247	N ₆	33
Murine calprotectin	0.525	0.158	0.30	248	N ₆	34
[Mn(H ₂ O) ₆] ²⁺ ^h	0.430-0.610	0-0.183	0-0.30	≈265	O ₆	22

^aThe sign of D is unknown unless reported with a + or - sign. Based on uncertainty in the linewidths, we estimate the error in our measurements to be ± 50 MHz (± 2.9 mT).

^bNitrogen ligands are backbone amides, histidines, or azide. Oxygen ligands are carboxylate groups or water derived.

^cMnSOD of *Deinococcus radiodurans*.

^dMnSOD of *Escherichia coli*.

^eOxalate decarboxylase of *Bacillus subtilis*.

^fMn lipoxygenase from *Gaemannomyces grammis*.

^gMulti-copper oxidase of *Bacillus* sp. PL-12 with substrate Mn(II) bound.

^hThe zero-field splitting parameters and ⁵⁵Mn hyperfine for [Mn(H₂O)₆]²⁺ depend on the ionic strength, buffer, and glassing agent as detailed in ref. 22.

ⁱn.d. = not determined.